Normal vibration modes and the structural phase transitions in caesium trichloroplumbate $CsPbCl_3$

1991 J. Phys.: Condens. Matter 3 1371

(http://iopscience.iop.org/0953-8984/3/11/002)

J. Phys.: Condens. Matter 3 (1991) 1371–1388. Printed in the UK

Normal vibration modes and the structural phase transitions in caesium trichloroplumbate $CsPbCl_3$

G L Hua

Department of Physics, Monash University, Clayton, Victoria, Australia

Received 28 June 1990, in final form 5 November 1990

Abstract. The perovskite crystal $CsPbCl_3$ is built up by a three-dimensional chain of $PbCl_6$ octahedra. The symmetry, the compatibility relation and the normal vibration modes of this crystal are studied by using the multiplier representation of group theory along the Γ–Δ–X–Z–M–T–R direction in phase I and along the Γ–Λ–Z direction in phase II. The successive structural phase transitions (SPT) in $CsPbCl_3$ at $T_{c1} = 47\,^{\circ}C$, $T_{c2} = 42\,^{\circ}C$ and $T_{c3} = 37\,^{\circ}C$ are induced by the condensation of the cubic zone boundary mode τ_3 at the M point and the tetragonal zone boundary modes τ_{9x} and τ_{9y} at the Z point separately. The interpretation of these successive displacive phase transitions with the normal vibration modes from our study is in good agreement with experimental investigation. A similar result from a previous investigation of layered perovskite $RbAlF_4$, which has a two-dimensional octahedral network, is also compared and discussed.

1. Introduction

The structure of the perovskite type crystals ABX_3 is built up by a three-dimensional (3D) array of BX_6 octahedra. Successive structural phase transitions, which are caused by the condensation of a specific zone centre and zone boundary phonon modes in the ideal cubic structure, have been observed in many perovskite crystals such as $BaTiO_3$, $PbTiO_3$, $KTaO_3$ [1], $SrTiO_3$ [2], $LaAlO_3$ [3], $KMnF_3$ [4] and $NaNbO_3$ [5]. The eigenvectors of the soft phonon modes, the amplitudes of which are small compared with the interatomic distances, correspond to the atomic displacements in the structure stabilized below the transition temperature T_c. As a result, the crystals transform into slightly distorted structures from the ideal cubic phase. Extensive investigations and considerable advances have been made on the understanding of these displacive structural phase transitions (SPT) in the past decade.

The perovskite crystals $CsPbCl_3$, $CsSrCl_3$, $RbCdCl_3$ and $CsPbBr_3$ exhibit a similar sequence of displacive SPT at different temperatures [6–9]. These displacive SPT are associated with various rotations of the relatively rigid octahedra, which are the results of the condensation of certain zone boundary modes at T_c. The non-ferroelectric crystal $CsPbCl_3$ undergoes a first order SPT at $T_{c1} = 47\,^{\circ}C$, a second order SPT at $T_{c2} = 42\,^{\circ}C$ and again a first order SPT at $T_{c3} = 37\,^{\circ}C$. This crystal has the ideal cubic perovskite structure with space group $Pm3m$ (O_h^1) in phase I. At T_{c1}, the condensed zone boundary mode τ_3 (M_3) at the M point $(\frac{1}{2}, \frac{1}{2}, 0)$ of the Brillouin zone produced the tilting of the octahedra BX_6 around the [001] axis and the new unit cell volume is doubled. Phase II is tetragonal with space group $P4/mbm$(D_{4h}^5). The second SPT at

0953-8984/91/111371+18$03.50

T_{c2} is associated with the softening of one of the doubly degenerate mode τ_{9x} (Z_{5x}) at the Z point $(0, 0, \frac{1}{2})$ of the tetragonal zone boundary. The mode τ_{9x} is generated from the triply degenerate mode τ_9 (R_{25}) at the R point $(\frac{1}{2}, \frac{1}{2}, \frac{1}{2})$ of the cubic structure and represents rotation of the octahedra BX_6 around the [100] axis of the cubic phase. Phase III is orthorhombic with space group $Cmcm$ (D_{2h}^{17}) and the unit cell volume is quadrupled with eight formula units of $CsPbCl_3$. The third SPT at T_{c3} is caused by the tilting of the octahedra BX_6 around the [010] cubic axis, and is associated with the softening of the zone boundary mode τ_{9y} (Z_{5y}) of the tetragonal phase. The space group of phase IV is $Pnma$ (D_{2h}^{16}) and the orthorhombic unit cell contains four formula units of $CsPbCl_3$. The data of this SPT sequence are listed in table 1 and the unit cells of the successive phases are shown in figure 1. Crystal dynamical investigations including neutron scattering studies into the phase transitions in $CsPbCl_3$ [6], in $CsSrCl_3$ [7] and in $CsPbBr_3$ [9], and a nuclear magnetic resonance (NMR) study into the SPT in $CsPbCl_3$ and $RbCdCl_3$ [8] are reported in the literature. In this paper we present a study into the symmetry and normal vibrations of $CsPbCl_3$ for both phases I and II by the multiplier representation of group theory [10] and a crystal dynamical interpretation of the successive displacive SPTs in $CsPbCl_3$. The mechanism of the phase transitions in $CsSrCl_3$, $RbCdCl_3$ and $CsPbBr_3$ are also included in our discussion.

Table 1. Structural data of $CsPbCl_3$ and $CsPbBr_3$, extracted from [6, 8, 9]. The space group of $CsPbCl_3$ in phase IV is $Pnma$ (D_{2h}^{16}) in [8] and $P2_1/m$ (C_{2h}^2) in [6] separately. The structural data and phase transition sequence in $CsSrCl_3$ and $RbCdCl_3$ correspond nearly completely to that of $CsPbCl_3$ [7, 8].

	Phase	T_c(°C)	Order	Soft mode	Space group	Axes in cubic system	Z
$CsPbCl_3$	I				$Pm3m$ (O_h^1)	[100] [010] [001]	1
		47	First	τ_3 (M_3)			
	II				$P4/mbm$ (D_{4h}^5)	[-110] [-1-10] [001]	2
		42	Second	τ_{9x} (Z_{5x})			
	III				$Cmcm$ (D_{2h}^{17})	[010] [-100] [001]	8
		37	First	τ_{9y} (Z_{5y})			
	IV				$Pnma$ (D_{2h}^{16})	[110] [001] [1-10]	4
$CsPbBr_3$	I				$Pm3m$ (O_h^1)	[100] [010] [001]	1
		130	First	τ_3 (M_3)			
	II				$P4/mbm$ (D_{4h}^5)	[110] [1-10] [001]	2
		88	Second	$\tau_{9x} + \tau_{9y}$ ($Z_{5x} + Z_{5y}$)			
	III				$Pnma$ (D_{2h}^{16})	[110] [1-10] [001]	4

2. Symmetry and the normal vibration modes of $CsPbCl_3$ in phases I and II

The symmetry properties, symmetry vibration modes and the compatibility relationships of $CsPbCl_3$ in phase II, along the Γ–Λ–Z direction in the Brillouin zone are calculated by using the multiplier representation of group theory [10] and presented in tables 3, 6 and figure 2. The symmetry nomenclature from Kovalev [11] we used are compared with notations from Fujii [6] in brackets where necessary. The condition for the compatibility of representations along a line of symmetry and a point lying on that

line is that the sum of the characters of the compatible representations should agree for the group of the wavevectors along that same line [12]. As for phase I, which is the ideal cubic perovskite structure, the symmetry properties and the normal vibration modes are well known and are available in the literature [17]. Therefore, we present here in tables 2 and 4 only the parts which are necessary in our discussion.

Table 2. Symmetry properties of $CsPbCl_3$ in phase I. Space group $Pm3m$ (O_h^1). (1). The little group and the symmetry species correspond to the individual wavevectors in the Brillouin zone are presented by Kovalev notation [11]. The nomenclature from Cowley [17] and Fujii [6] are also listed in brackets in tables 1 and 2 for comparison. (2) The degeneracies of the symmetry modes are presented in tables 4 and 6. (3) $0.0 < \mu < 0.5$.

	k vector	Little group	Symmetry species of the normal modes
Γ	k_{12} (0,0,0)	T205	$\tau_8+4\tau_{10}$ $(\Gamma_{25} + 4\Gamma_{15})$
Δ	k_8 $(\mu,0,0)$	T119	$4\tau_1 + \tau_3 + 5\tau_5$ $(4\Delta_1 + \Delta_2 + 5\Delta_5)$
X	k_{10} (0.5,0,0)	T147	$2\tau_1 + 2\tau_4 + \tau_8 + 2\tau_9 + 3\tau_{10}$ $(2M_2' + 2M_1 + M_3 + 2M_5' + 3M_5)$
Z	k_6 $(0.5,\mu,0)$	T11	$5\tau_1 + 2\tau_2 + 3\tau_3 + 5\tau_4$ $(5\Sigma_3 + 2\Sigma_4 + 3\Sigma_2 + 5\Sigma_1)$
M	k_{11} (0.5,0.5,0)	T147	$\tau_1 + \tau_3 + 2\tau_4 + \tau_5 + \tau_6 + \tau_7 + \tau_9 + 3\tau_{10}$ $(M_4 + M_3 + 2M_3' + M_2 + M_2' + M_1 + M_5 + 3M_5')$
T	k_7 $(0.5,0.5,\mu)$	T119	$3\tau_1 + \tau_2 + \tau_3 + 2\tau_4 + 4\tau_5$ $(3\Delta_2' + \Delta_2 + \Delta_1' + 2\Delta_1 + 4\Delta_5)$
R	k_{13} (0.5,0.5,0.5)	T205	$\tau_1 + \tau_5 + 2\tau_7 + \tau_9 + \tau_{10}$ $(\Gamma_2' + \Gamma_{12}' + 2\Gamma_{15} + \Gamma_{25} + \Gamma_{25}')$

Table 3. Symmetry properties of $CsPbCl_3$ in phase II. Space group $P4/mbm$ (D_{4h}^5). Notes as for table 2.

	k vector	Little group	Symmetry species of the normal modes
Γ	k_{17} (0,0,0)	T147	$\tau_1 + 2\tau_2 + \tau_3 + 4\tau_4 + \tau_5$ $+ 2\tau_6 + \tau_7 + \tau_9 + 8\tau_{10}$
Δ	k_{13} $(0,0,\mu)$	T119	$5\tau_1 + 3\tau_2 + \tau_3 + 3\tau_4 + 9\tau_5$
Z	k_{19} (0,0,0.5)	T147	$3\tau_1 + \tau_2 + 2\tau_3 + 2\tau_4 + \tau_5$ $+ \tau_6 + 2\tau_7 + 5\tau_9 + 4\tau_{10}$ $(3Z_1 + Z_1' + 2Z_2 + Z_3 + Z_3'$ $+ 2Z_4 + 2Z_4' + 5Z_5 + 4Z_5')$

The normal vibration modes at the zone centre of phase I are calculated from the symmetry eigenvectors (table 4) by using further unitary transformation and are presented in table 5. The twelve non-acoustic phonon modes are grouped into four triply degenerate modes, each of which includes three orthogonal modes along the cubic principal axes [100], [010] and [001] respectively. They are illustrated in figure 3 and can be described in the following way.

(i) The τ_8 mode represents the opposite bendings of the Cl–Pb–Cl bonds of the octahedra. The Cl ions which are in the (001) (or (100) and (010)) plane vibrate

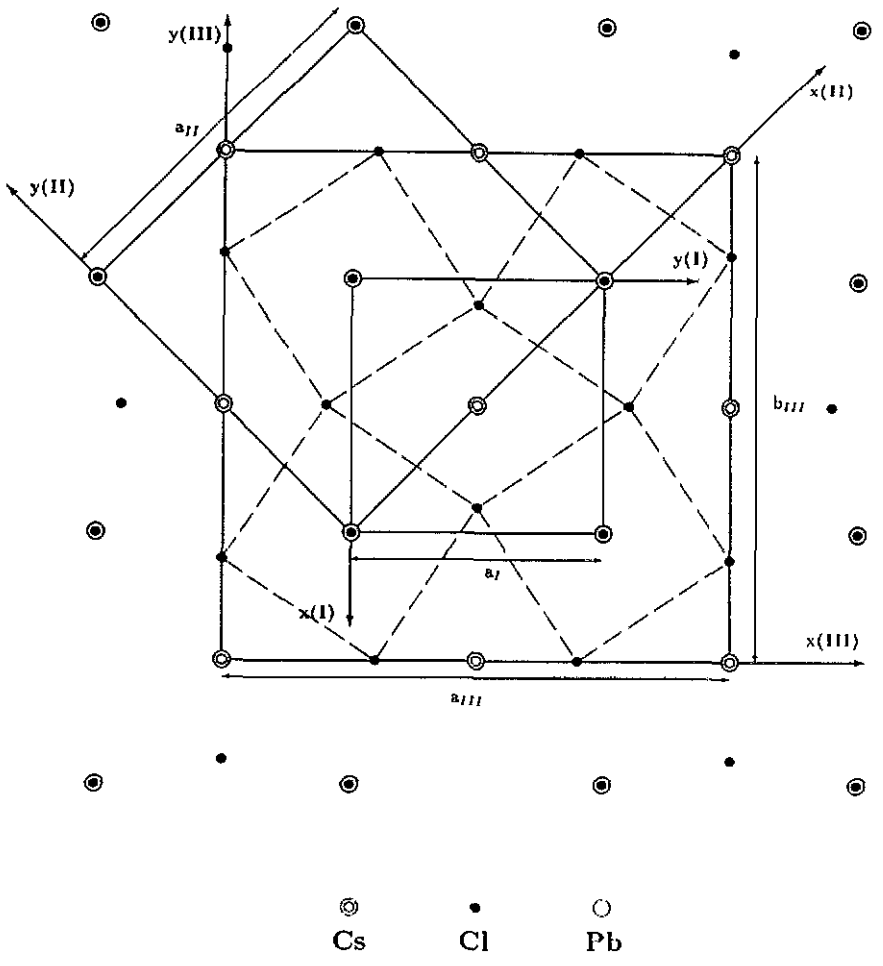

Figure 1. The unit cell projections onto the (001) plane of $CsPbCl_3$ in phases I, II and III.

against each other along the [001] direction, while the Cl ions on the [001] axis do not move at all.

(ii) One of the τ_{10} mode describes the distortion of the octahedra BX_6 which is produced by the vibration of all the Cl ions. The bending of the Cl–Pb–Cl bonds is caused by the Cl ions in the (001) (or (100) and (010)) plane all of which move along the same [001] direction, while other Cl ions on the [001] axis will move in opposite direction and result in the stretching and sqeezing of the Cl–Pb bonds.

(iii) Another τ_{10} mode involves the relative translational motion of the cubic lattice, including the Cs and Pb ions, and the sublattice formed by the 3D octahedral network. The resultant motion of these vibrations is the asymmetric stretching of the Cl–Pb bonds along the three principal axes.

(iv) The last τ_{10} mode has the vibration pattern of the relative translational motion of the cubic sublattices formed by the Cs and Pb ions.

In a previous paper [13] we investigated the normal vibrations and SPT in the layered perovskite $RbAlF_4$. This has a layer structure with a 2D array of octahedra

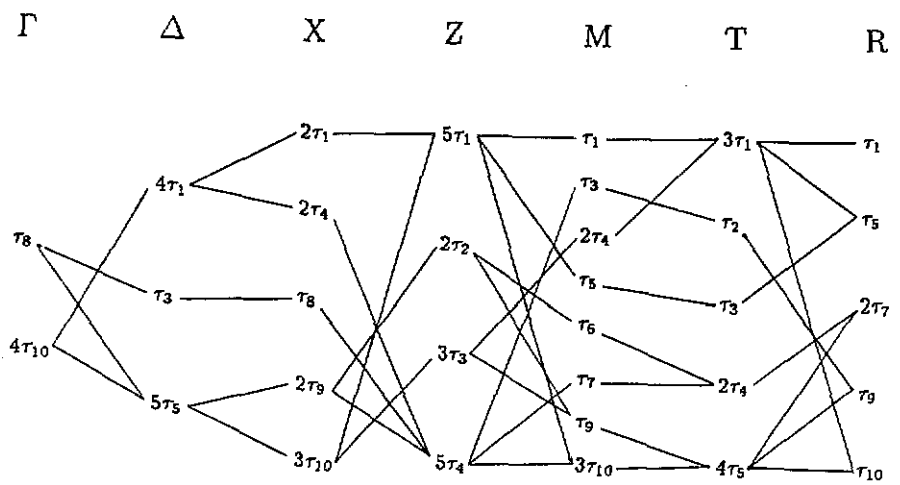

(a)

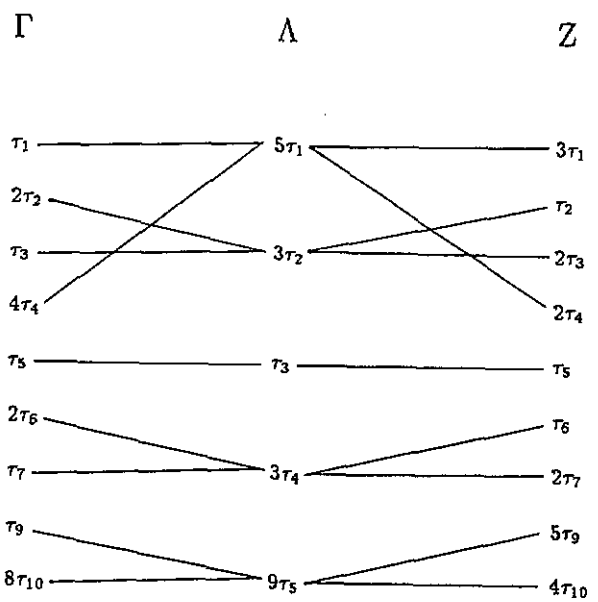

(b)

Figure 2. The compatibility relations along (*a*) the symmetry direction Γ–Δ–X–Z–M–T–R in phase I and (*b*) along the Γ–Λ–Z *direction in* phase II.

Table 4. Symmetry vibration modes of $CsPbCl_3$ in phase I. Space group $Pm3m$ (O_h^1). The Cl_{eq} ions are in the equatorial (001) plane and the Cl_{ax} ions are along the [001] axis. The τ_3 (M_3) mode of the M point is condensed at T_{c1}, while the softening of the τ_9 (R_{25}) mode at the R point induced the SPT at T_{c2} and T_{c3}

Γ	Cs	Pb	Cl_1,Cl_2(Cl_{eq})	Cl_3 (Cl_{ax})
τ_8			$x_2 - x_3$	
			$y_1 - y_3$	
			$z_1 - z_2$	
τ_{10}	X	X	$x_2 + x_3$	x_1
	Y	Y	$y_1 + y_3$	y_2
	Z	Z	$z_1 + z_2$	z_3

M	Cs	Pb	Cl_1,Cl_2(Cl_{eq})	Cl_3 (Cl_{ax})
τ_1			$x_1 + y_2$	
τ_3			$y_1 - x_2$	
τ_4		Z		z_3
τ_5			$x_1 - y_2$	
τ_6	Z			
τ_7			$y_1 + x_2$	
τ_9			z_1	
			z_2	
τ_{10}	X	X		x_3
	Y	Y		y_3

R	Cs	Pb	Cl_1,Cl_2(Cl_{eq}), Cl_3 (Cl_{ax})
τ_1			$x_1 + y_2 + z_3$
τ_5			$x_1 + y_2 - 2z_3$
			$x_1 - y_2$
τ_7	X		$z_2 + y_3$
	Y		$z_1 + x_3$
	Z		$y_1 + x_2$
τ_9			$z_2 - y_3$
			$z_1 - x_3$
			$y_1 - x_2$
τ_{10}		X	
		Y	
		Z	

AlF_6, in contrast to $CsPbCl_3$ which is built up by a 3D network of $PbCl_6$ octahedra. It is interesting to compare the results from these two crystals in our discussion. The layer perovskite $RbAlF_4$ has a tetragonal symmetry with space group $P4/mmm(D_{4h}^1)$ in phase I. The fifteen non-acoustic modes at the zone centre are divided into five groups. Among them four groups have almost the same vibration patterns as those in $CsPbCl_3$. However, as a result of the tetragonal symmetry, each group of vibrations splits from a triply degenerate mode in $CsPbCl_3$ into a doubly degenerate mode in the (001) plane and a singly degenerate mode along the [001] axis in $RbAlF_4$. The physically identical Cl ions in the cubic $CsPbCl_3$ split into Cl_{eq} ions which are in the equatorial (001) plane and Cl_{ax} ions which lie on the [001] axis. The equivalence of the motion of the Cl ions along the three cubic axes no longer exists in $RbAlF_4$. As a

Table 5. Normal vibration modes of $CsPbCl_3$ in phase I at the zone centre Γ.

τ_8	T_{2u}	$(1/\sqrt{2})(x_2 - x_3)$
		$(1/\sqrt{2})(y_1 - y_3)$
		$(1/\sqrt{2})(z_1 - z_2)$
τ_{10}	T_{1u}	$(1/\sqrt{5})(X_{Cs} + X_{Pb} + x_1 + x_2 + x_3)$
		$(1/\sqrt{5})(Y_{Cs} + Y_{Pb} + y_1 + y_2 + y_3)$
		$(1/\sqrt{5})(Z_{Cs} + Z_{Pb} + z_1 + z_2 + z_3)$
		$(1/\sqrt{2})(X_{Cs} - X_{Pb})$
		$(1/\sqrt{2})(Y_{Cs} - Y_{Pb})$
		$(1/\sqrt{2})(Z_{Cs} - Z_{Pb})$
		$(1/\sqrt{6})[(x_2 + x_3) - 2x_1]$
		$(1/\sqrt{6})[(y_1 + y_3) - 2y_2]$
		$(1/\sqrt{6})[(z_1 + z_2) - 2z_3]$
		$(\sqrt{2/15})[\frac{3}{2}(X_{Cs} + X_{Pb}) - (x_1 + x_2 + x_3)]$
		$(\sqrt{2/15})[\frac{3}{2}(Y_{Cs} + Y_{Pb}) - (y_1 + y_2 + y_3)]$
		$(\sqrt{2/15})[\frac{3}{2}(Z_{Cs} + Z_{Pb}) - (z_1 + z_2 + z_3)]$

Table 6. Symmetry vibration modes of $CsPbCl_3$ in phase II. Space group $P4/mbm$ (D^5_{4h}).

Γ		Cs_1, Cs_2	Pb_1, Pb_2	Cl_1,Cl_2,Cl_3,Cl_4(Cl_{eq})	Cl_5,Cl_6(Cl_{ax})
τ_1	A_{1g}			$x_1 - y_1 + x_2 + y_2 - x_3 - y_3 - x_4 + y_4$	
$2\tau_2$	A_{1u}		$Z_1 - Z_2$		$z_5 - z_6$
τ_3	A_{2g}			$x_1 + y_1 - x_2 + y_2 + x_3 - y_3 - x_4 - y_4$	
$4\tau_4$	A_{2u}	$Z_1 + Z_2$	$Z_1 + Z_2$	$z_1 + z_2 + z_3 + z_4$	$z_5 + z_6$
τ_5	B_{1g}			$x_1 + y_1 + x_2 - y_2 - x_3 + y_3 - x_4 - y_4$	
$2\tau_6$	B_{1u}	$Z_1 - Z_2$		$z_1 - z_2 - z_3 + z_4$	
τ_7	B_{2g}			$x_1 - y_1 - x_2 - y_2 + x_3 + y_3 - x_4 + y_4$	
τ_9	E_g			$z_1 - z_2 + z_3 - z_4$	
				$z_1 + z_2 - z_3 - z_4$	
$8\tau_{10}$	E_u	$X_1 + X_2$	$X_1 + X_2$	$x_1 + y_1 + x_2 + y_2 + x_3 + y_3 + x_4 + y_4$	$x_5 + x_6$
		$Y_1 + Y_2$	$Y_1 + Y_2$	$x_1 - y_1 + x_2 - y_2 + x_3 - y_3 + x_4 - y_4$	$y_5 + y_6$
		$X_1 - X_2$	$X_1 - X_2$	$x_1 + y_1 - x_2 - y_2 - x_3 - y_3 + x_4 + y_4$	$x_5 - x_6$
		$Y_1 - Y_2$	$Y_1 - Y_2$	$x_1 - y_1 - x_2 + y_2 - x_3 + y_3 + x_4 - y_4$	$y_5 - y_6$

Z	Cs_1, Cs_2	Pb_1, Pb_2	Cl_1,Cl_2,Cl_3,Cl_4(Cl_{eq})	Cl_5,Cl_6(Cl_{ax})
$3\tau_1$	$Z_1 + Z_2$		$x_1 - y_1 + x_2 + y_2 - x_3 - y_3 - x_4 + y_4$	$z_5 + z_6$
τ_2		$Z_1 - Z_2$		
$2\tau_3$			$x_1 + y_1 - x_2 + y_2 + x_3 - y_3 - x_4 - y_4$	$z_5 - z_6$
$2\tau_4$		$Z_1 + Z_2$	$z_1 + z_2 + z_3 + z_4$	
τ_5			$x_1 + y_1 + x_2 - y_2 - x_3 + y_3 - x_4 - y_4$	
τ_6			$z_1 - z_2 - z_3 + z_4$	
$2\tau_7$	$Z_1 - Z_2$		$x_1 - y_1 - x_2 - y_2 + x_3 + y_3 - x_4 + y_4$	
$5\tau_9$	$X_1 + X_2$			$x_5 + x_6$
	$X_1 - X_2$		$z_1 - z_2 + z_3 - z_4$	$x_5 - x_6$
	$Y_1 - Y_2$		$z_1 + z_2 - z_3 - z_4$	$y_5 - y_6$
	$Y_1 + Y_2$			$y_5 + y_6$
$4\tau_{10}$		$X_1 + X_2$	$x_1 + y_1 + x_2 + y_2 + x_3 + y_3 + x_4 + y_4$	
		$Y_1 + Y_2$	$x_1 - y_1 + x_2 - y_2 + x_3 - y_3 + x_4 - y_4$	
		$X_1 - X_2$	$x_1 + y_1 - x_2 - y_2 - x_3 - y_3 + x_4 + y_4$	
		$Y_1 - Y_2$	$x_1 - y_1 - x_2 + y_2 - x_3 + y_3 + x_4 - y_4$	

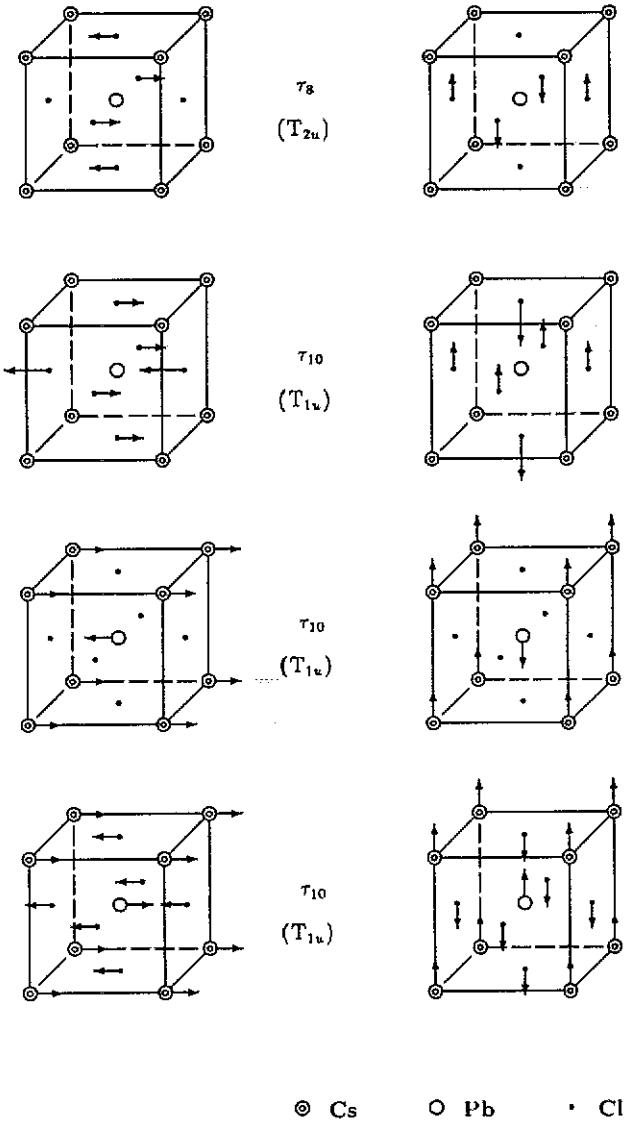

Figure 3. The normal vibration modes of $CsPbCl_3$ in phase I at the zone centre Γ. Vibrations along the [100] and [001] directions of each triply degenerate mode are presented.

result, the cubic τ_8 mode generates into tetragonal $\tau_8 + \tau_{10}$ modes, and the opposite vibrations of the Cl ions along three cubic axes are replaced by the opposite vibrations of the Cl_{eq} ions only. Similarly, the cubic τ_{10} mode, which includes the vibrations of all the Cl ions, changed into tetragonal $\tau_4 + \tau_{10}$ modes, and the Cl_{eq} and Cl_{ax} ions always move against each other. Another group of vibrations in $RbAlF_4$, which comes from the characteristic layer structure and describes the relative motion of the F_{ax} ions, does not exist in $CsPbCl_3$. Other evidence of the characteristic layer structure in $RbAlF_4$ obtained from a previous investigation [13], such as the consistency of symmetry and symmetry vibrations along M–V–A (the [001] axis) and the anisotropy

of compatibility relations along [001] and along [100] and [010] axes in phase I, also do not appear in $CsPbCl_3$ (table 2 and figure 2). Despite all these differences, the small dispersion of the phonon branches along the $[\frac{1}{2},\frac{1}{2},0]$–$[\frac{1}{2},\frac{1}{2},\frac{1}{2}]$ direction in phase I, which is the driving force of the successive SPT, exists in both crystals [6,14]. In $CsPbCl_3$, the softening of the τ_3 (M_3) mode, the eigenvector of which is y_1-x_2 in table 4 and represents the rotation of the octahedra around the [001] axis, is responsible for the displacive SPT at T_{c1}. The τ_9 (R_{25}) mode, with eigenvectors z_2-y_3, x_1-x_3 and y_1-x_2 in table 4, describes the rotation of the octahedra around the three cubic principal axes. The R point $(\frac{1}{2},\frac{1}{2},\frac{1}{2})$ of the cubic phase transforms into the Z point $(0,0,\frac{1}{2})$ of the tetragonal phase. As a result, the R_{25} mode is modified under the influence of the tetragonality and splits into a singly degenerate mode τ_1 and a doubly degenerate mode $\tau_{9x}+\tau_{9y}$ ($Z_1+Z_{5x}+Z_{5y}$) in phase II. The τ_1 mode is accompanied by the displacements of both ions Cs and Cl_{ax} along the [001] direction, while the τ_9 mode is associated with displacements of the Cs ions along the rotation axes of the octahedra (see table 6). The condensation of the τ_{9x} and τ_{9y} mode lead to the displacive SPT at T_{c2} and T_{c3} separately. The difference between the M_3 and the R_{25} modes is that the R_{25} mode represents the opposite rotation of the neighboring BX_6 octahedra along the rotation axis, whereas the M_3 mode represents the rotation in the same direction.

The 30 symmetry eigenvectors at the zone centre of $CsPbCl_3$ in phase II are listed in table 6. They can be divided into four groups. The first group, which includes six eigenvectors $\tau_4+\tau_6+2\tau_{10}$, consists of the relative vibration and translational motion of the two tetragonal sublattices formed by the Cs_1 and Cs_2 ions. Another six modes $\tau_2+\tau_4+2\tau_{10}$ describe the same kind of motion for the Pb_1 and Pb_2 sublattices as those in the first group. The motion of the Cl_{eq} ions are given by 12 of the modes. Among them eight modes are in the equatorial plane, which are $\tau_1+\tau_3+\tau_5+\tau_7+2\tau_{10}$, and four of them $\tau_4+\tau_6+\tau_9$ are along the [001] axis. The modes τ_1,τ_3,τ_5 and τ_7, describe the tilting, stretching, sqeezing and twisting of the octahedra around the [001] axis in the equatorial plane. One of the τ_{10} modes represents the bending of the Cl_{eq}–Pb–Cl_{eq} bonds while another τ_{10} mode corresponds to the translational motion of the 3D octahedra array in the (001) plane. These symmetry vibration patterns are illustrated in figure 4. During the SPT at T_{c1}, the M point of the cubic reciprocal lattice is transformed into the Γ point of the tetragonal lattice. As a result, the symmetry modes τ_1, τ_3, τ_5 and τ_7 show the same vibration patterns as τ_3, τ_1, τ_5 and τ_7 modes at the M point of phase I, and thus can be regarded as originated from them. It is the eigenvector τ_1 (A_{1g}) here exhibits a soft mode behaviour as phase I is approached *from temperature below* T_{c1} , *and should be assigned to the soft mode for the* SPT at T_{c1} [14]. The four modes $\tau_4+\tau_6+\tau_9$, which involve the vibrations along the [001] axis of the Cl_{eq} ions, are the translational (τ_4), the Cl_{eq}–Pb–Cl_{eq} bond bending (τ_6), and the tilting of the octahedra around the [100] and [010] axes (τ_9). The last group of 6 eigenvectors describe the 3D translation and relative vibrations of Cl_{ax} ions from the neighbouring octahedra in the (001) plane. The phase II of $CsPbCl_3$ and $RbAlF_4$ are both tetragonal with the same space group of D_{4h}^5. Naturally, the 30 symmetry species and symmetry vibration modes at the zone centre for $CsPbCl_3$ and $RbAlF_4$ should be identical (some little differences from slightly different linear combinations). The six extra modes $\tau_1+\tau_3+2\tau_9$ in $RbAlF_4$, which emerge from the layer structure and involve the relative vibrations of F_{ax} ions in the same octahedra, do not exist in $CsPbCl_3$.

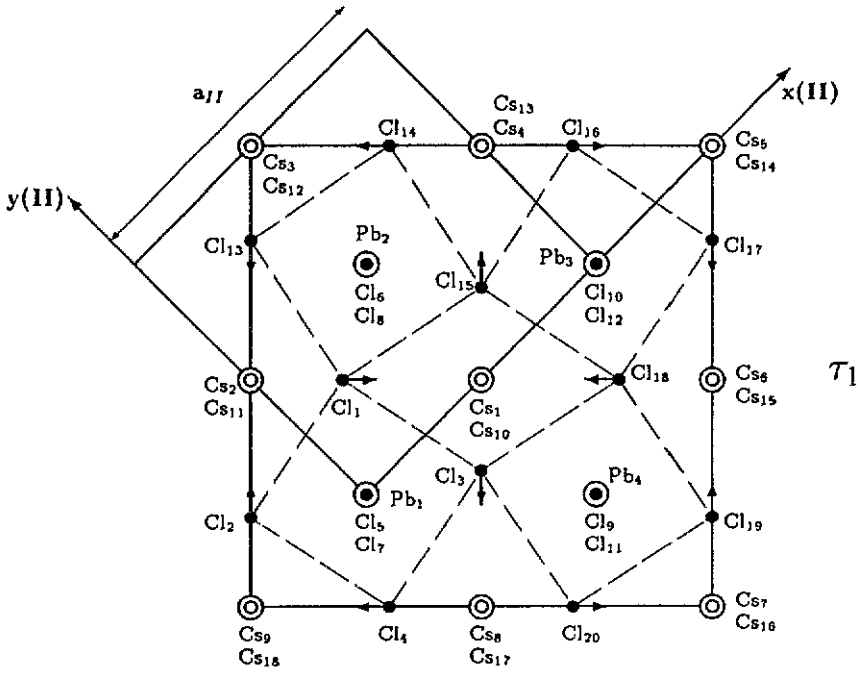

τ_1 (A_{1g})

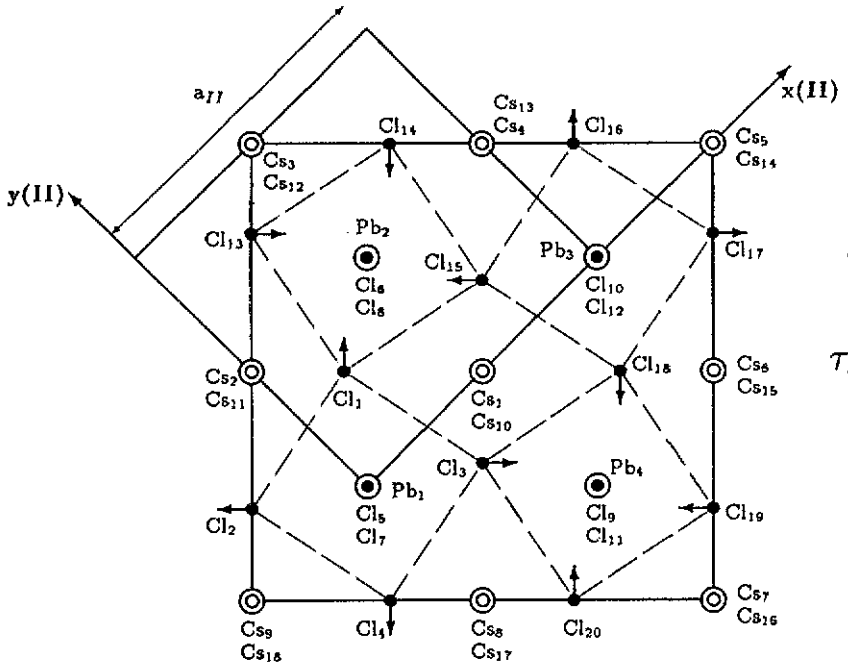

τ_3 (A_{2g})

Figure 4. The symmetry vibration modes of $CsPbCl_3$ at the zone centre Γ in phase II. Only those representing the motion of Cl_{eq} ions in the (001) plane are presented.

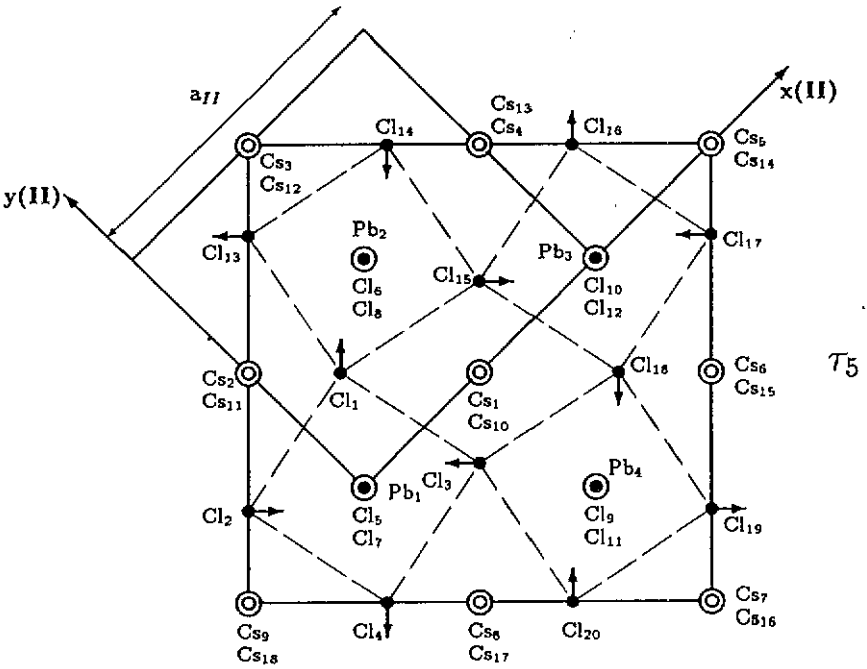

τ_5 (B_{1g})

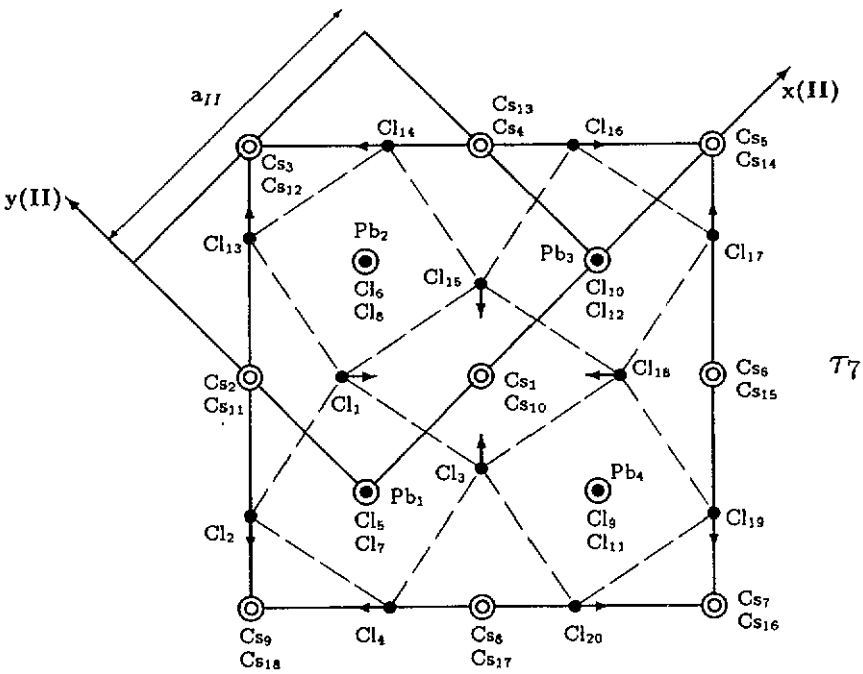

τ_7 (B_{2g})

Figure 4. (Continued)

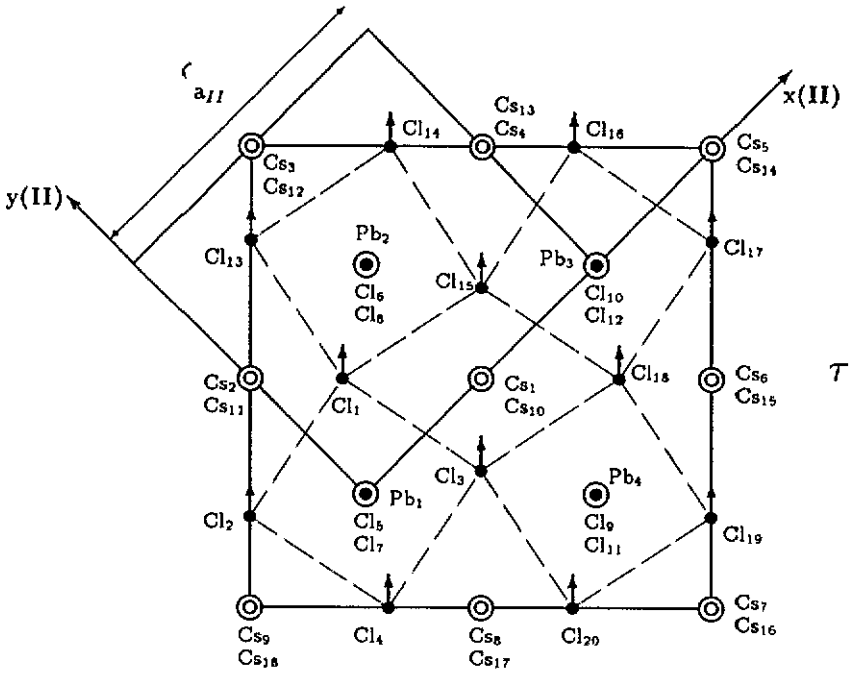

$\tau_{10}\ (E_u)$

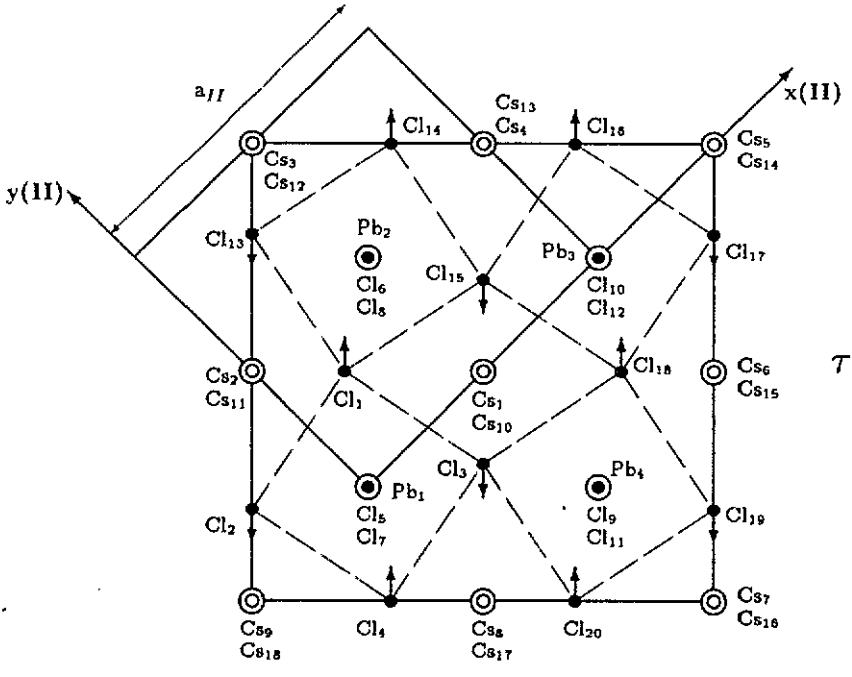

$\tau_{10}\ (E_u)$

Figure 4. (Continued)

3. The interpretation of the SPT at T_{c1} T_{c2} and T_{c3} from the normal vibration modes

The detailed structural data of $CsPbCl_3$ is given by Fujii [6] and Alexandrov [15]. The unit cell of phase I, II and III, which are cubic, tetragonal and orthorhombic respectively, are illustrated in figure 1. The unit cell parameters are related to each other as

$$\begin{aligned} &a_{III} = \sqrt{2}a_{II} = 2a_I \qquad b_{III} = \sqrt{2}b_{II} = 2b_I \qquad c_{III} = 2c_{II} = 2c_I \\ &(a_I = b_I) \qquad (a_{II} = b_{II}) \qquad (a_{III} \simeq b_{III}). \end{aligned} \tag{1}$$

The first-order phase transition at T_{c1} in $CsPbCl_3$ is induced by the softening of the τ_3 (M_3) mode in the Brillouin zone. The eigenvector of this mode $[y_1 - x_2]$, which involves only the motion of the Cl_{eq} atoms in the equatorial plane (table 4), gives exactly the tilting of the octahedra around the [001] axis which stimulated this displacive phase transition.

The second order SPT at T_{c2} is caused by the tilt of the $PbCl_6$ octahedra around the [100] cubic axis and accompanied by displacements of the Cs ions along the same direction [6]. This is associated with the condensation of τ_{9x} mode at the Z point $(0, 0, \frac{1}{2})$ in the tetragonal Brillouin zone. This displacive phase transition can be explained in the following way. As a result of the condensed mode, the atomic displacement $\boldsymbol{U}_{l\kappa}(\boldsymbol{r}_l)$, which describes the displacement of the κth atom in the lth unit cell from its equilibrium position, can be written as

$$\boldsymbol{U}_{l\kappa}(\boldsymbol{r}_l) = Q_{\boldsymbol{k}} \boldsymbol{e}_\kappa(\boldsymbol{k}) \exp(\mathrm{i}\boldsymbol{k} \cdot \boldsymbol{r}_l). \tag{2}$$

Here $Q_{\boldsymbol{k}}$ is a complex normal mode coordinate, $\boldsymbol{e}_\kappa(\boldsymbol{k})$ is the eigenvector of the soft mode and $\boldsymbol{r}_l$ is the position vector of the atoms in the lth unit cell. For simplicity we assume that the phase of the complex coordinate $\Theta_{\boldsymbol{k}} = 0$. In phase II, the position vector $\boldsymbol{r}_{l\kappa}$ of the κth atom in the lth unit cell is given by

$$\boldsymbol{r}_{l\kappa} = \boldsymbol{r}^0_{l\kappa} + \boldsymbol{U}_{l\kappa}. \tag{3}$$

The vectors $\boldsymbol{r}^0_{l\kappa}$ in equation (3), which stand for the atomic equilibrium positions in the exact tetrahedral structure of phase II, are listed in the first column in table 7. These vectors $\boldsymbol{r}^0_{l\kappa}$ are further transformed into the corresponding orthorhombic unit cell of phase III with the following equations and are presented in the second column of the same table.

$$\begin{aligned} x_{III} &= \tfrac{1}{2}x_{II} - \tfrac{1}{2}y_{II} + \tfrac{1}{4} \\ y_{III} &= \tfrac{1}{2}x_{II} + \tfrac{1}{2}y_{II} + \tfrac{1}{4} \\ z_{III} &= \tfrac{1}{2}z_{II} + \tfrac{1}{2}. \end{aligned} \tag{4}$$

The third column of table 7 gives the (c), (d), (e), (f) and (g) sites of the orthorhombic unit cell ($Cmcm$,D^{17}_{2h}) which should be occupied by the atoms under equilibrium in phase III. These sites are represented by $\boldsymbol{r}_{l\kappa}$ in equation (3). During the SPT at T_{c2}, the condensation of the mode τ_{9x} at $\boldsymbol{k} = (0, 0, \frac{1}{2})$ will provide the necessary displacements $\boldsymbol{U}_{l\kappa}$ in (3) for each atom to move from its regular positions $\boldsymbol{r}^0_{l\kappa}$ in phase II (column

2, table 7) to its new equilibrium position $r_{l\kappa}$ in phase III (column 3, table 7). These displacements are predicted by comparing column 2 and column 3 and listed in column 4 in the same table. By using suitable linear combination of the doubly degenerate mode τ_9 derived from our normal vibration analysis (table 6), we are able to further calculate these expected displacements.

The displacements of the Cs ions along the [100] cubic axis, which is the [010] direction for the orthorhombic unit cell in figure 1, are obtained by recombining the doubly degenerate mode τ_9 in table 6 into $\tau_{9x} : -(X_1 + Y_1), (X_2 + Y_2); \tau_{9y} : -(X_1 - Y_1), (X_2 - Y_2)$. These displacements are in the tetragonal unit cell and should be transformed into the orthorhombic lattice according to equation (4). Supposing that X and Y have equal magnitude σ, we derive the displacements for Cs ions as

$$\begin{array}{llllll} \tau_{9x}: & \text{Cs1} & \delta x = 0 & \delta y = -\sigma & \delta z = 0 \\ & \text{Cs2} & \delta x = 0 & \delta y = \sigma & \delta z = 0 \\ \tau_{9y}: & \text{Cs1} & \delta x = -\sigma & \delta y = 0 & \delta z = 0 \\ & \text{Cs2} & \delta x = \sigma & \delta y = 0 & \delta z = 0. \end{array} \tag{5}$$

The parameter σ has not been determined [15]. The displacements of other Cs ions, which are not in the same tetragonal unit cell, can be calculated in the same way by considering the corresponding position vectors r_l^0 and wave vector $(0, 0, \frac{1}{2})$ in equation (2). In column 3 of table 7 only atoms of one half of the orthorhombic unit cell are listed. The other half of the unit cell lies on top or below of the first half along the z axis. As a result of equation (2), the displacements of atoms, belonging to the upper or lower half of the orthorhombic unit cell, have opposite displacements than those in column 3. The results are in overall agreement with the expectation from column 4 of table 7.

There are no dynamical displacements for the Pb ions which are the centres of the rigid octahedra during the phase transformation. The transition displacements of the Cl_{eq} ions are similarly given by rearranging the doubly degenerate mode τ_9 into $\tau_{9x} : -(z2 - z3); \tau_{9y} : (z1 - z4)$. Here τ_{9x} and τ_{9y} represent the rotation of the octahedra around the cubic [100] and [010] axes respectively. Using equation (4) and assuming $z = 2\alpha$, we derived

$$\begin{array}{llllll} \tau_{9x}: & \text{Cl1} & \delta x = 0 & \delta y = 0 & \delta z = 0 \\ & \text{Cl2} & \delta x = 0 & \delta y = 0 & \delta z = -\alpha \\ & \text{Cl3} & \delta x = 0 & \delta y = 0 & \delta z = \alpha \\ & \text{Cl4} & \delta x = 0 & \delta y = 0 & \delta z = 0 \\ \tau_{9y}: & \text{Cl1} & \delta x = 0 & \delta y = 0 & \delta z = \alpha \\ & \text{Cl2} & \delta x = 0 & \delta y = 0 & \delta z = 0 \\ & \text{Cl3} & \delta x = 0 & \delta y = 0 & \delta z = 0 \\ & \text{Cl4} & \delta x = 0 & \delta y = 0 & \delta z = -\alpha. \end{array} \tag{6}$$

The parameter $\alpha = 0.049a_{\text{III}}$ is the result of the tilting angle $\phi = 11°$ of the octahedra around the [100] cubic axis at T_{c2} [15]. Although the parameter γ in column 1 and 3 of table 7 both represent the rotation of the octahedra around the [001] axis in phase II and III, the rotation angles are different. In phase II the tilting angle $\psi = 4.3°$ and $\gamma = 0.019a_{\text{II}}$, while in phase III $\psi = 6.1°$ and $\gamma = 0.027a_{\text{III}}$ [15]. Detailed analysis

Table 7. Atomic parameters of $CsPbCl_3$ in phases II and III. The first and second column in the table present the equilibrium atomic positions $r^0_{l\kappa}$ in phase II, referred to the tetrahedral (D^5_{4h}) and the orthorhombic (D^{17}_{2h}) unit cell respectively. The third column gives the $r_{l\kappa}$ values of the (c), (d), (e), (f) and (g) sites of the orthorhombic unit cell in phase III. The expected atomic displacements $U_{l\kappa}$ during the SPT at T_{c2} are listed in the last column. The parameter γ (= 0.019 in the first and second columns) is the result of the rotation angle $\psi = 4.3°$ around the [001] cubic axis in phase II. The same parameter γ (= 0.027 in the third column) represents the tilting angle $\psi = 6.1°$ in phase III [15]. The parameter α (= 0.049) is produced by the rotation of the octahedra around the [100] cubic axis with angle $\phi = 11°$ [15]. The parameters β and σ have not been measured and determined.

	Phase II. D^5_{4h}	Phase II. D^{17}_{2h}	Phase III. D^{17}_{2h}	u_x, u_y, u_z
Cs_1	$\frac{1}{2},0,\frac{1}{2}$	$\frac{1}{2},\frac{1}{2},\frac{3}{4}$	$\frac{1}{2},\frac{1}{2}-\sigma,\frac{3}{4}$	$0,-\sigma,0$
Cs_2	$0,\frac{1}{2},\frac{1}{2}$	$0,\frac{1}{2},\frac{3}{4}$	$0,\frac{1}{2}+\sigma,\frac{3}{4}$	$0,\sigma,0$
Cs_3	$\frac{1}{2},1,\frac{1}{2}$	$0,1,\frac{3}{4}$	$0,1-\sigma,\frac{3}{4}$	$0,-\sigma,0$
Cs_4	$1,\frac{1}{2},\frac{1}{2}$	$\frac{1}{2},1,\frac{3}{4}$	$\frac{1}{2},1+\sigma,\frac{3}{4}$	$0,\sigma,0$
Cs_5	$\frac{3}{2},0,\frac{1}{2}$	$1,1,\frac{3}{4}$	$1,1-\sigma,\frac{3}{4}$	$0,-\sigma,0$
Cs_6	$1,-\frac{1}{2},\frac{1}{2}$	$1,\frac{1}{2},\frac{3}{4}$	$1,\frac{1}{2}+\sigma,\frac{3}{4}$	$0,\sigma,0$
Cs_7	$\frac{1}{2},-1,\frac{1}{2}$	$1,0,\frac{3}{4}$	$1,-\sigma,\frac{3}{4}$	$0,-\sigma,0$
Cs_8	$0,-\frac{1}{2},\frac{1}{2}$	$\frac{1}{2},0,\frac{3}{4}$	$\frac{1}{2},\sigma,\frac{3}{4}$	$0,\sigma,0$
Cs_9	$-\frac{1}{2},0,\frac{1}{2}$	$0,0,\frac{3}{4}$	$0,-\sigma,\frac{3}{4}$	$0,-\sigma,0$
Cs_{10}	$\frac{1}{2},0,-\frac{1}{2}$	$\frac{1}{2},\frac{1}{2},\frac{1}{4}$	$\frac{1}{2},\frac{1}{2}+\sigma,\frac{1}{4}$	$0,\sigma,0$
Cs_{11}	$0,\frac{1}{2},-\frac{1}{2}$	$0,\frac{1}{2},\frac{1}{4}$	$0,\frac{1}{2}-\sigma,\frac{1}{4}$	$0,-\sigma,0$
Cs_{12}	$\frac{1}{2},1,-\frac{1}{2}$	$0,1,\frac{1}{4}$	$0,1+\sigma,\frac{1}{4}$	$0,\sigma,0$
Cs_{13}	$1,\frac{1}{2},-\frac{1}{2}$	$\frac{1}{2},1,\frac{1}{4}$	$\frac{1}{2},1-\sigma,\frac{1}{4}$	$0,-\sigma,0$
Cs_{14}	$\frac{3}{2},0,-\frac{1}{2}$	$1,1,\frac{1}{4}$	$1,1+\sigma,\frac{1}{4}$	$0,\sigma,0$
Cs_{15}	$1,-\frac{1}{2},-\frac{1}{2}$	$1,\frac{1}{2},\frac{1}{4}$	$1,\frac{1}{2}-\sigma,\frac{1}{4}$	$0,-\sigma,0$
Cs_{16}	$\frac{1}{2},-1,-\frac{1}{2}$	$1,0,\frac{1}{4}$	$1,\sigma,\frac{1}{4}$	$0,\sigma,0$
Cs_{17}	$0,-\frac{1}{2},-\frac{1}{2}$	$\frac{1}{2},0,\frac{1}{4}$	$\frac{1}{2},-\sigma,\frac{1}{4}$	$0,-\sigma,0$
Cs_{18}	$-\frac{1}{2},0,-\frac{1}{2}$	$0,0,\frac{1}{4}$	$0,\sigma,\frac{1}{4}$	$0,\sigma,0$
Pb_1	$0,0,0$	$\frac{1}{4},\frac{1}{4},\frac{1}{2}$	$\frac{1}{4},\frac{1}{4},\frac{1}{2}$	$0,0,0$
Pb_2	$\frac{1}{2},\frac{1}{2},0$	$\frac{1}{4},\frac{3}{4},\frac{1}{2}$	$\frac{1}{4},\frac{3}{4},\frac{1}{2}$	$0,0,0$
Pb_3	$1,0,0$	$\frac{3}{4},\frac{3}{4},\frac{1}{2}$	$\frac{3}{4},\frac{3}{4},\frac{1}{2}$	$0,0,0$
Pb_4	$\frac{1}{2},-\frac{1}{2},0$	$\frac{3}{4},\frac{1}{4},\frac{1}{2}$	$\frac{3}{4},\frac{1}{4},\frac{1}{2}$	$0,0,0$
Cl_1	$\frac{1}{4}-\gamma,\frac{1}{4}+\gamma,0$	$\frac{1}{4}-\gamma,\frac{1}{2},\frac{1}{2}$	$\frac{1}{4}-\gamma,\frac{1}{2},\frac{1}{2}$	$0,0,0$
Cl_2	$-\frac{1}{4}-\gamma,\frac{1}{4}-\gamma,0$	$0,\frac{1}{4}-\gamma,\frac{1}{2}$	$0,\frac{1}{4}-\gamma,\frac{1}{2}-\alpha$	$0,0,-\alpha$
Cl_3	$\frac{1}{4}+\gamma,\gamma-\frac{1}{4},0$	$\frac{1}{2},\frac{1}{4}+\gamma,\frac{1}{2}$	$\frac{1}{2},\frac{1}{4}+\gamma,\frac{1}{2}+\alpha$	$0,0,\alpha$
Cl_4	$\gamma-\frac{1}{4},-\frac{1}{4}-\gamma,0$	$\frac{1}{4}+\gamma,0,\frac{1}{2}$	$\frac{1}{4}+\gamma,0,\frac{1}{2}$	$0,0,0$
Cl_5	$0,0,\frac{1}{2}$	$\frac{1}{4},\frac{1}{4},\frac{3}{4}$	$\frac{1}{4}-\alpha,\frac{1}{4}-\beta,\frac{3}{4}$	$-\alpha,-\beta,0$
Cl_6	$\frac{1}{2},\frac{1}{2},\frac{1}{2}$	$\frac{1}{4},\frac{3}{4},\frac{3}{4}$	$\frac{1}{4}+\alpha,\frac{3}{4}-\beta,\frac{3}{4}$	$\alpha,-\beta,0$
Cl_7	$0,0,-\frac{1}{2}$	$\frac{1}{4},\frac{1}{4},\frac{1}{4}$	$\frac{1}{4}+\alpha,\frac{1}{4}+\beta,\frac{1}{4}$	$\alpha,\beta,0$
Cl_8	$\frac{1}{2},\frac{1}{2},-\frac{1}{2}$	$\frac{1}{4},\frac{3}{4},\frac{1}{4}$	$\frac{1}{4}-\alpha,\frac{3}{4}+\beta,\frac{1}{4}$	$-\alpha,\beta,0$
Cl_9	$\frac{1}{2},-\frac{1}{2},\frac{1}{2}$	$\frac{3}{4},\frac{1}{4},\frac{3}{4}$	$\frac{3}{4}+\alpha,\frac{1}{4}-\beta,\frac{3}{4}$	$\alpha,-\beta,0$
Cl_{10}	$1,0,\frac{1}{2}$	$\frac{3}{4},\frac{3}{4},\frac{3}{4}$	$\frac{3}{4}-\alpha,\frac{3}{4}-\beta,\frac{3}{4}$	$-\alpha,-\beta,0$
Cl_{11}	$\frac{1}{2},-\frac{1}{2},-\frac{1}{2}$	$\frac{3}{4},\frac{1}{4},\frac{1}{4}$	$\frac{3}{4}-\alpha,\frac{1}{4}+\beta,\frac{1}{4}$	$-\alpha,\beta,0$
Cl_{12}	$1,0,-\frac{1}{2}$	$\frac{3}{4},\frac{3}{4},\frac{1}{4}$	$\frac{3}{4}+\alpha,\frac{3}{4}+\beta,\frac{1}{4}$	$\alpha,\beta,0$
Cl_{13}	$\frac{1}{4}+\gamma,\frac{3}{4}+\gamma,0$	$0,\frac{3}{4}+\gamma,\frac{1}{2}$	$0,\frac{3}{4}+\gamma,\frac{1}{2}+\alpha$	$0,0,\alpha$
Cl_{14}	$\frac{3}{4}+\gamma,\frac{3}{4}-\gamma,0$	$\frac{1}{4}+\gamma,1,\frac{1}{2}$	$\frac{1}{4}+\gamma,1,\frac{1}{2}$	$0,0,0$
Cl_{15}	$\frac{3}{4}-\gamma,\frac{1}{4}-\gamma,0$	$\frac{1}{2},\frac{3}{4}-\gamma,\frac{1}{2}$	$\frac{1}{2},\frac{3}{4}-\gamma,\frac{1}{2}-\alpha$	$0,0,-\alpha$
Cl_{16}	$\frac{5}{4}-\gamma,\frac{1}{4}+\gamma,0$	$\frac{3}{4}-\gamma,1,\frac{1}{2}$	$\frac{3}{4}-\gamma,1,\frac{1}{2}$	$0,0,0$
Cl_{17}	$\frac{5}{4}+\gamma,\gamma-\frac{1}{4},0$	$1,\frac{3}{4}+\gamma,\frac{1}{2}$	$1,\frac{3}{4}+\gamma,\frac{1}{2}+\alpha$	$0,0,\alpha$
Cl_{18}	$\frac{3}{4}+\gamma,-\frac{1}{4}-\gamma,0$	$\frac{3}{4}+\gamma,\frac{1}{2},\frac{1}{2}$	$\frac{3}{4}+\gamma,\frac{1}{2},\frac{1}{2}$	$0,0,0$
Cl_{19}	$\frac{3}{4}-\gamma,-\frac{3}{4}-\gamma,0$	$1,\frac{1}{4}-\gamma,\frac{1}{2}$	$1,\frac{1}{4}-\gamma,\frac{1}{2}-\alpha$	$0,0,-\alpha$
Cl_{20}	$\frac{1}{4}-\gamma,\gamma-\frac{3}{4},0$	$\frac{3}{4}-\gamma,0,\frac{1}{2}$	$\frac{3}{4}-\gamma,0,\frac{1}{2}$	$0,0,0$

using equation (2) showed that this increase of the rotation angle from phase II to III should be the result of further softening of the τ_3 (M_3) mode at the cubic zone boundary or the τ_1 mode at the tetragonal zone centre, but not the τ_1 mode at the tetragonal Z point $(0, 0, \frac{1}{2})$ which leads to a contradiction with the structural data in phase III.

The displacements of the Cl_{ax} atoms are calculated in the following way. The eigenvectors of the doubly degenerate mode τ_{9x} and τ_{9y} in table 6 are recombined as τ_{9x}: x_5, y_5; and τ_{9y}: x_6, y_6. Further, assuming weak anisotropy, we transform the symmetry modes into

$$\tau_{9x} : -(Q_1 x_5 - Q_2 y_5), (Q_2 x_6 - Q_1 y_6) \qquad \tau_{9y} : -(Q_1 x_5 + Q_2 y_5), (Q_2 x_6 + Q_1 y_6) \tag{7}$$

in which $Q_1 \simeq Q_2, Q_1 > Q_2$. Assuming $x = y = 2\epsilon$, we further transform these soft mode displacements into the orthorhombic lattice as

$$\begin{array}{lllll}
\tau_{9x}: \text{Cl5} & \delta x = -\epsilon(Q_1 + Q_2) = -\alpha & \delta y = \epsilon(Q_2 - Q_1) = -\beta & \delta z = 0 \\
\text{Cl6} & \delta x = \epsilon(Q_1 + Q_2) = \alpha & \delta y = \epsilon(Q_2 - Q_1) = -\beta & \delta z = 0 \\
\tau_{9y}: \text{Cl5} & \delta x = -\epsilon(Q_1 - Q_2) = -\beta & \delta y = -\epsilon(Q_1 + Q_2) = -\alpha & \delta z = 0 \\
\text{Cl6} & \delta x = \epsilon(Q_2 - Q_1) = -\beta & \delta y = \epsilon(Q_1 + Q_2) = \alpha & \delta z = 0.
\end{array} \tag{8}$$

Using equation (2), we can calculate all the expected displacements for Cl_{ax} ions in table 7. The parameter $\epsilon(Q_1 + Q_2) = \alpha = 0.049 a_{III}$ is the result of the tilting of the octahedra around the cubic [100] axis and the parameter β has not been determined [15].

From the crystal chemical point of view [16], the B ions of the ABX_3 crystal in the cubic phase are tightly restricted in the space left by the anions, while the A ions are accommodated more spaciously. The cell parameter is practically independent of the R_A and is smaller than the sum of R_B and R_X. This indicates strong interaction of the B–X bonds. The tension of the B–X bond increases with the falling temperature, and constitutes one of the chief reasons for the SPT in ABX_3. The rotations of the BX_6 octahedra around the cubic principal axes not only changes the A–X distance but may also be accompanied by slight increments of the B–X distance, relieving the state of stress. The interaction of the Pb–Cl bond plays a more important role in changing the crystal symmetry from cubic ($a_I = b_I$) to tetragonal and orthorhombic ($a_{III} \neq b_{III}$ and $a_{III} \simeq b_{III}$). Therefore, we have applied the anisotropy of the soft mode displacements in the (001) plane to Cl_{ax} ions but not to Cs ions in our calculation.

The SPT at T_{c3} is induced by the softening of the τ_{9y} mode at the Z point of the tetragonal structure. The condensation of this mode is associated with another tilting of the octahedra around the [010] axis of the cubic cell and the displacements of the Cs ions along the same axis. The space group of phase IV is given as $P2_1/m$ (C_{2h}^2) [6] and $Pnma$ (D_{2h}^{16}) [8] from different investigations. At present the detailed structural data are not available. However, we can still discuss the atomic displacements, induced by the soft mode τ_{9y} from our normal vibration calculation. According to Fujii [6] and Plesko [8] the condensed doubly degenerate mode τ_{9x} and τ_{9y} have the same displacive amplitude. The Cl_{eq} ions in phase III, including Cl_1 (Cl_4) and Cl_2 (Cl_3),

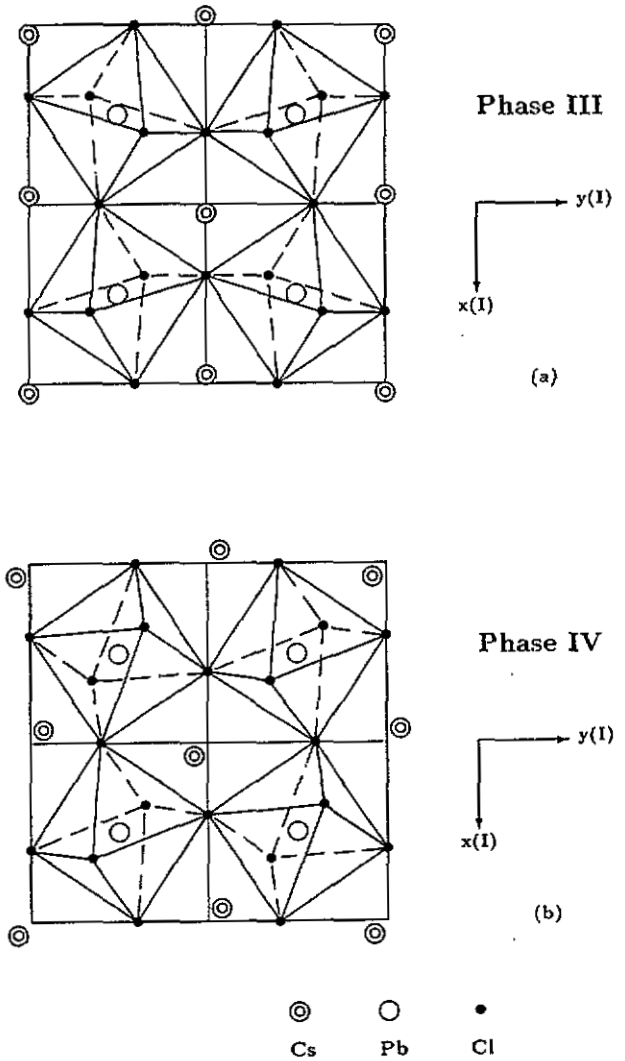

Figure 5. The crystal orthorhombic structure of $CsPbCl_3$ at (*a*) phase III and (*b*) phase IV, schematically drawn from equations (5), (6) and (8). The Pb ions are placed on the $z = \frac{1}{2}$ plane and the Cs ions are placed on the $z = \frac{3}{4}$ plane. The Cs ions on the $z = \frac{1}{4}$ plane, which are not shown in the figure, have opposite displacements.

become crystallographically non-equivalent. The Cl_2 ions shift out of the (001) plane containing the Pb ions, while the Cl_1 ions are placed nearly on its plane, this results in the environment around the Cl_1 and Cl_2 ions being substantially different. In phase IV the Cl_1 (Cl_4) also shifts out of the original (001) plane, while Cl_2 (Cl_3) stays at nearly the same position as in phase III. The ionic arrangements around the two ions were found to be very similar, though not crystallographically equivalent, to each other. The Cl_{ax} ions also shift to new positions due to the rotation of the octahedra. As a result of all these changes, the direction of the rotation vector of the octahedra $PbCl_6$,

as well as the displacements of the Cs ions, will be pointing to the [110] axis of the cubic lattice [6]. The description of the displacements of the ions in phases III and IV agree well with equations (5), (6) and (8). The crystal structures of the successive phases III and IV, figure 5, from our normal vibration analysis, show the same patterns as those predicted by Fujii [6] and Plesko [8]. The interpretation of the successive SPTs in $CsPbCl_3$ is in good agreement with the result of the experimental investigation.

The structure, the symmetry and the successive SPT in $CsSrCl_3$ and $RbCdCl_3$ correspond nearly completely to those of $CsPbCl_3$ [7,8]. Therefore, the discussion for $CsPbCl_3$ should also be valid for $CsSrCl_3$ and $RbCdCl_3$. The sequence of SPT in $CsPbBr_3$ has some differences (see table 1). The mechanism of the SPT from cubic (O_h^1) to tetragonal (D_{4h}^5) structure at $T_{c1} = 130\,^{\circ}C$ is the same as that of $CsPbCl_3$. The second order SPT at $T_{c2} = 88\,^{\circ}C$ is different. Instead of the condensed mode τ_{9x} in $CsPbCl_3$, the transition is induced by the condensation of the doubly degenerate mode $\tau_{9x} + \tau_{9y}$. Previous investigation on $CsPbBr_3$ showed [18] that in phase III each Pb ion is surrounded by six Br ions, which form a distorted octahedra, and five of these Br ions are shared by two or even three octahedra, so that they form bridges between the Pb ions. The result of this is the transformation of a 3D octahedral network in phase II into a structure of extended chains of Pb–Br octahedra parallel to the a axis of the orthorhombic unit cell in phase III. The Cs ions are distributed between these chains of polynuclear complexes, and has a coordinate of 9 with the Br ions. The atomic distances change considerably and the crystal is thus disordered. There is no simple relationship between the unit cell parameter and the lattice planes of the two phases. The SPT at T_{c2} cannot be interpreted straightforwardly from the eigenvectors of the condensed mode $\tau_{9x} + \tau_{9y}$. Further experimental investigation should be carried out, so as to achieve a better understanding of the SPT in $CsPbBr_3$.

References

[1] Shirane G 1971 *Structural Phase Transitions and Soft Modes* ed E J Samuelson *et al* (Oslo: Universitetsforlaget)
[2] Shirane G and Yamada Y 1969 *Phys. Rev.* 177 858
[3] Axe J D, Shirane G and Müller K A 1969 *Phys. Rev.* 183 1256
[4] Minkiewicz V J, Fujii Y and Yamada Y 1970 *J. Phys. Soc. Japan* 28 443
[5] Ishida K and Honjo G 1973 *J. Phys. Soc. Japan* 34 1279
[6] Fujii Y, Hoshino S, Yamada Y and Shirane G 1974 *Phys. Rev.* B 9 4549
[7] Prokert F 1981 *Phys. Status Solidi* b 104 261
[8] Plesko S, Kind R and Roos J 1978 *J. Phys. Soc. Japan* 45 553
[9] Hirotsu S, Harada J, Iizumi M and Gesi K 1974 *J. Phys. Soc. Japan* 37 1393
[10] Maradudin A A and Vosko S H 1968 *Rev. Mod. Phys.* 40 1
[11] Kovalev O V 1965 *Irreducible Representations of the Space Group* (New York: Gordon and Breach)
[12] Slater J C 1965 *Quantum Theory of Molecular Solids* (New York: McGraw-Hill)
[13] Hua G L 1989 *J. Phys.: Condens. Matter* 1 9301
[14] Bulou A, Rousseau M, Nouet J, Loyzance P L, Mokhlisse R and Couzi M 1983 *J. Phys. C: Solid State Phys.* 16 4527
[15] Alexandrov K S, Besnosikov B V and Posdnjakova L A 1976 *Ferroelectrics* 12 197
[16] Alexandrov K S 1976 *Sov. Phys.-Crystallogr.* 21 133
[17] Cowley R A 1964 *Phys. Rev.* A 134 981
[18] Marstrander A and Møller C K 1966 *Mat. Fys. Meddr. Dansk. Vidensk. Selsk.* 35 No 5